J. Fluid Mech. (2008), *vol.* 611, *pp.* 151–173.
doi:10.1017/S0022112008002735 Printed in the United Kingdom

Nonlinear problem of flat-plate entry into an incompressible liquid

ODD M. FALTINSEN AND YURIY A. SEMENOV

Centre for Ship and Ocean Structures, NTNU, N-7491 Trondheim, Norway

(Received 21 May 2007 and in revised form 11 May 2008)

The self-similar flow and free-surface shape induced by a flat plate entering an inviscid and incompressible liquid are investigated for arbitrary initial conditions. An analytical solution, which is based on two governing expressions, namely the complex velocity and the derivative of the complex potential, is obtained. These expressions are derived in an auxiliary parameter plane using integral formulae proposed for the determination of an analytical function from its modulus and argument given on the boundary of the parameter region. We derive a system of an integral and an integro-differential equation in terms of the velocity modulus and the velocity angle at the free surface, which are determined by the dynamic and kinematic boundary conditions. A numerical procedure for solving these equations is carefully validated by comparisons with results available in the literature. The results are presented in terms of the free surface shape, the angles at the tip of the splash jet, the contact angles at the intersection with the plate surface, pressure distribution and force coefficients. New features caused by the flow unsteadiness are found and discussed.

1. Introduction

During the last decade, practical needs in the design of seaplanes, half-submerged propellers, planing hulls and high-speed vessels have lead to a renewal of interest in research on unsteady hydrodynamic effects which may lead to heavy hydrodynamic loads on the vessels and their structural elements (Faltinsen, Landrini & Greco 2004; Faltinsen 2005).

Water entry problems, a subset of general unsteady fluid-structure interaction problems, have been studied most for the case of wedge entry, to understand the phenomenon of slamming characterized by the formation of thin 'jets' running up the sides of the impacting wedge-shaped body and the occurrence of a high pressure peak near the core of the jets. For the oblique water entry of thin arbitrarily oriented wedges, flow separation may occur at the wedge apex. In this case only one side of the wedge interacts with the liquid and the flow corresponds to the water entry of a flat plate. This type of flow is characterized by an additional feature on the free surface: the formation of a splash jet running upwards but away from the plate.

A linear theory of the water entry of a flat plate has been developed by Wang (1977, 1979), to estimate unsteady loads on the blades of partially submerged propellers. Wang considered three stages of blade motion in the liquid, namely the initial, completely submerged and exit stages, and presented a linear solution for each stage. Using Sohotsky–Plemel's formula, the solution is derived in terms of the complex potential and integral equations for the determination of the vertical velocity component on the cavity boundary. However, linear theories of water entry problems

fail to predict the phenomenon of slamming, which is a result of coupled nonlinear and unsteady effects at relatively large incidence angles.

Nonlinear solutions of unsteady free-surface flows have been obtained only for a limited number of special cases, and they are based on the calculus of complex variables introduced in hydrodynamics by Helmholtz (1868). The first complete solution of this kind was obtained by Dobrovol'skaya (1969) for a two-dimensional symmetric wedge vertically entering the free surface at a constant entry speed. Dobrovol'skaya was able to reduce the problem to finding Wagner's function defined on the whole real axis of the upper half-plane, which is determined using the Schwarz integral formula. Chekin (1989) generalized Dobrovol'skaya's approach to the solution of the problems of water entry of a wedge and a flat plate. At the same time, instead of finding Wagner's function, Chekin represented, in integral form, the derivative of the function $z(u)$ which conformally maps the auxiliary upper half-plane u onto the flow region plane. He also introduced the function $\chi(u) = z'(u)V'(u)$ where $V(u)$ is the complex velocity (primes denote differentiation) and showed that $\mathrm{Im}\,[\chi(u)] = 0$ on the wetted part of the plate and $\mathrm{Re}\,[\chi(u)] = 0$ on the free boundaries. Using the Schwarz and Sohotsky–Plemel integral formulae, he found the relation between the argument and modulus of the function $z'(u)$. By taking advantage of the flow self-similarity and the boundary conditions, he reduced the problem to an integral equation in the unknown function $\arg[z'(u)]$. Chekin presented only one example of calculations, that for the case of the oblique entry of a flat plate. Other initial conditions are still to be investigated.

There are many publications concerning the water entry of blunt wedges and the normal impact of a flat plate based on various simplified methods or asymptotic expansions where use is made of Wagner's idea (Wagner 1932) of considering the water entry process as a sequence of impulse impacts. The problem was considered in the modern framework of matched asymptotic expansions by Cointe & Armand (1987), Wilson (1989), Howison, Ockendon & Wilson (1991), Mei, Liu & Yue (1999), Iafrati & Korobkin (2004), Howison, Ockendon & Oliver (2004), Oliver (2007).

In this paper we present a nonlinear analytical solution of the unsteady self-similar flow induced by the oblique water entry of a flat plate. The method of solution is based on further development of Chaplygin's singular point method, which is an extension of the hodograph method, and aimed at simplifying the determination of the analytical function that is the complex potential of a free-boundary flow. An example of the application of Chaplygin's singular point method to the derivation of analytical functions is presented in the paper by Semenov & Iafrati (2006) for the case of water entry of asymmetric wedges. By using this approach, it is possible to derive generalized formulae determining an analytical function from its boundary conditions of various kinds, which are presented in this paper (equations (2.5) and (2.9)). The advantage of these formulae is that an analytical function satisfying given boundary conditions is found directly without recourse to the singular point method.

Formula (2.5) determines an analytical function from its modulus and argument given on the imaginary and real axes of the first quadrant, which is chosen as the parameter region. Formula (2.9) determines an analytical function whose argument is given on both the real and imaginary axes. These formulae provide some simplification in solving nonlinear free-boundary problems because the dynamic (Cauchy–Lagrange integral) and the kinematic (non-penetration condition) boundary conditions directly determine the modulus and argument of the complex velocity.

Following Zhukovskii's method (Zhukovskii 1890), the solution is given in terms of two governing functions, which are the complex velocity and the derivative of

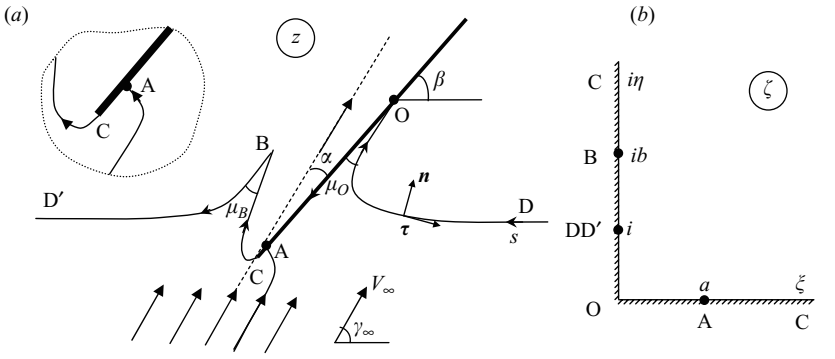

FIGURE 1. Sketch of the initial stage of flat plate water entry: (*a*) the physical plane, (*b*) the parameter plane.

the complex potential defined in the first quadrant of the parameter plane. The theoretical formulation of the problem discussed in § 2 is similar to that presented for the self-similar water entry problem for asymmetric wedges (Semenov & Iafrati 2006). Attention is given to a new type of singularity, which appears in the expression for the derivative of the complex potential due to the corner point of the splash jet on the free surface. The integral representation of the complex velocity contains a function which is the velocity modulus along the free boundary. The integral representation of the derivative of the complex potential contains a function which is the angle the velocity vector forms with the free surface. Both the velocity modulus and the angle of the velocity vector are functions of a parameter variable along the imaginary axis of the first quadrant. The solution is obtained in the form of a system of an integral and an integro-differential equation in the aforementioned functions, which are derived from the dynamic and kinematic boundary conditions using the self-similar statement of the problem. In § 3, a numerical method for solving the system of integral equations is presented. It is carefully validated by comparing the results obtained with those of Wang's (1977, 1979) linear theory and Chekin's (1989) nonlinear theory. In § 4, the results for the oblique entry of a flat plate are presented in terms of the free surface shape, the contact angle of the tip jet, the angle of the splash jet on the free surface, pressure distributions and force coefficients.

2. Theoretical formulation and analysis

The initial stage of the entry of a flat plate into water with free surface originally at rest is studied in a frame of reference attached to the impacting body with its origin C located at the leading edge of the flat plate. The wetted part of the plate OC is less than the length of the plate. In this frame of reference, away from the plate the fluid velocity is directed along a line forming an angle γ_∞ with the horizontal axis x, and its modulus approaches the value V_∞ (see figure 1*a*). The liquid is assumed to be incompressible, and gravity, surface tension and viscous effects are neglected. The pressure on the free surface is constant and equal to the atmospheric pressure. Let α denote the angle of attack relative to the velocity direction, $\beta = \gamma_\infty - \alpha$ is the deadrise angle.

A feature of the problem is the presence of a corner point, B, on the free surface. At time $t = 0$ points B, O and the leading edge of the flat plate are located at the same point of the undisturbed free surface. For $t > 0$ the initial free surface that existed at time $t = 0$ and the 'new' free surface starting from the leading edge of the flat

plate are governed by the same equation of motion $\boldsymbol{a} = -\mathrm{grad}\, P$ where $\boldsymbol{a}$ is the liquid particle acceleration, and P is the pressure in the liquid. If the pressure on the free surface is constant and lower than the pressure in the liquid, then the acceleration is in the direction of the outer normal vector of the free surface. The same direction of acceleration of a liquid particle moving along either the initial or 'new' free surface can result in only concave shapes of these parts of the free surface. The junction of the initial and 'new' concave free surfaces leads to the corner point B. We note that a liquid particle at point B does not move along the free surface because it moves with the tip of the splash jet. This point separates the total free surface into two concave lines. The corner point B is a result of interaction of the undisturbed free surface and the flat plate at time $t = 0$. Only one such point exists. Owing to the flow self-similarity, there are no other corner points on the free surface for $t > 0$. Existing experiments confirm this flow topology.

For a constant entry velocity, the time-dependent problem in the physical plane $Z = X + \mathrm{i}Y$ can be written in terms of the self-similar variables in the stationary region $x = X/(V_0 t)$, $y = Y/(V_0 t)$ where V_0 is the velocity modulus at the contact point O in the physical plane.

According to the above definitions, V_0 is used as a reference value, and then the velocity modulus of point O in the stationary plane is unity ($v_0 = 1$). The complex velocity potential $W(Z, t) = \Phi(Z, t) + \mathrm{i}\Psi(Z, t)$ takes the form

$$W(Z, t) = V_0^2 t\, w(z) = V_0^2 t\, [\phi(z) + \mathrm{i}\psi(z)]\,. \tag{2.1}$$

The problem is to determine a function $w(z)$ which conformally maps the stationary plane z onto the complex velocity potential region w. As pointed by Zhukovskii (1890), it is easier to find mapping functions in parametric form using an auxiliary parameter plane. Following Chaplygin (his method is discussed in the book by Gurevich 1965), we choose the first quadrant of the ς-plane as the parameter region corresponding to the flow region to derive expressions for the complex velocity, $\mathrm{d}w/\mathrm{d}z$, and the derivative of the complex potential, $\mathrm{d}w/\mathrm{d}\varsigma$, as functions of the variable $\varsigma = \xi + \mathrm{i}\eta$. If these functions are known, the velocity field and the relation between the parameter region and the physical flow region can be determined as follows:

$$v_x - \mathrm{i}v_y = \frac{\mathrm{d}w}{\mathrm{d}z}(\varsigma), \quad z(\varsigma) = z(0) + \int_0^{\varsigma} \frac{\mathrm{d}w}{\mathrm{d}\varsigma} \Big/ \frac{\mathrm{d}w}{\mathrm{d}z}\, \mathrm{d}\varsigma, \tag{2.2}$$

where v_x and v_y are the x- and y-components of the velocity.

Conformal mapping allows us to fix three arbitrary points in the parameter region, which are O, C and D as shown in figure 1(*b*). In this plane, the positive imaginary axis ($\eta > 0,\ \xi = 0$) corresponds to the free surface and the positive real axis ($\xi > 0,\ \eta = 0$) corresponds to the wetted part of the plate.

The points $\varsigma = a$ and $\varsigma = \mathrm{i}b$ are the images of the stagnation point A and the tip B of the splash jet in the physical plane, respectively. The parameters a and b are unknowns and have to be determined as part of the solution.

2.1. *Expressions for the complex velocity and for the derivative of the complex potential*

At this stage it is assumed that the velocity modulus along the free surface, that is along the positive part of the imaginary axis,

$$v(\eta) = \left| \frac{\mathrm{d}w}{\mathrm{d}z} \right| \tag{2.3}$$

is known. This function will be determined below using the dynamic boundary condition. In the frame of reference attached to the flat plate, the normal velocity component equals zero due to the impermeability condition. This means that the argument χ of the complex velocity along the real axis of the parameter region is fixed and determined by the plate orientation

$$\chi(\xi) = \arg(\mathrm{d}w/\mathrm{d}z) = \begin{cases} -\beta, & 0 < \xi < a, \quad \eta = 0 \\ -\pi - \beta, & a < \xi < \infty, \quad \eta = 0. \end{cases} \tag{2.4}$$

The problem is then to find a function $\mathrm{d}w/\mathrm{d}z$ in the first quadrant of the parameter plane which satisfies the given boundary conditions. The formula

$$\frac{\mathrm{d}w}{\mathrm{d}z} = v(\infty)\exp\left[\frac{1}{\pi}\int_0^\infty \frac{\mathrm{d}\chi}{\mathrm{d}\xi'}\ln\left(\frac{\varsigma+\xi'}{\varsigma-\xi'}\right)\mathrm{d}\xi' - \frac{\mathrm{i}}{\pi}\int_0^\infty \frac{\mathrm{d}\ln v}{\mathrm{d}\eta'}\ln\left(\frac{\varsigma-\mathrm{i}\eta'}{\varsigma+\mathrm{i}\eta'}\right)\mathrm{d}\eta' + \mathrm{i}\chi(\infty)\right] \tag{2.5}$$

provides a solution of the mixed boundary-value problem in the first quadrant of the complex plane ς. It can be easily verified that for $\varsigma = \xi$ the argument of the function $\mathrm{d}w/\mathrm{d}z$ is the function $\chi(\xi)$ while for $\varsigma = \mathrm{i}\eta$ the modulus of $\mathrm{d}w/\mathrm{d}z$ is the function $v(\eta)$, i.e. the boundary conditions (2.3) and (2.4) are satisfied. Some specific cases of this integral formula were obtained when solving the problems of a free boundary flow in a corner-shaped Hele-Shaw cell (Semenov & Cummings 2006) and of the self-similar asymmetric entry of a wedge into water (Semenov & Iafrati 2006).

The argument of the complex velocity undergoes a step change at the point $\varsigma = a$ corresponding to the splitting of the streamline at the stagnation point A in the physical plane. Substituting equation (2.4) into the first integral in (2.5) and taking into account that $\arg(\varsigma - \mathrm{i}\eta') = \arg(\mathrm{i}\eta' - \varsigma) - \pi$ in the second integral, we finally obtain an expression for the complex velocity in the ς-plane as

$$\frac{\mathrm{d}w}{\mathrm{d}z} = \left(\frac{\varsigma - a}{\varsigma + a}\right)\exp\left[-\frac{\mathrm{i}}{\pi}\int_0^\infty \frac{\mathrm{d}\ln v}{\mathrm{d}\eta'}\ln\left(\frac{\mathrm{i}\eta' - \varsigma}{\mathrm{i}\eta' + \varsigma}\right)\mathrm{d}\eta' - \mathrm{i}(\pi + \beta)\right]. \tag{2.6}$$

This expression shows that the complex velocity function has only one simple zero corresponding to the stagnation point A.

In order to analyse the behaviour of the velocity potential along the free surface, it is useful to introduce the unit vectors $\boldsymbol{n}$ and $\boldsymbol{\tau}$ which are normal and tangent to the free surface, respectively. The normal vector is directed from the fluid region outward while the spatial coordinate along the free surface s increases along the free surface with the fluid region on the left (figure 1). With this notation,

$$\mathrm{d}w = (v_s + \mathrm{i}v_n)\,\mathrm{d}s, \tag{2.7}$$

where v_s and v_n are the tangential and normal velocity components, respectively. Let θ denote the angle between the velocity vector on the free surface and the unit vector $\boldsymbol{\tau}$, $\theta = \tan^{-1}\left(v_n/v_s\right)$; its behaviour along the boundary of the fluid region is shown in figure 2.

The definition (2.7) allows us to determine the argument of the derivative of the complex potential $\mathrm{d}w/\mathrm{d}\varsigma$ which appears in equation (2.2),

$$\vartheta(\varsigma) = \arg\left(\frac{\mathrm{d}w}{\mathrm{d}\varsigma}\right) = \arg\left(\frac{\mathrm{d}w}{\mathrm{d}s}\right) + \arg\left(\frac{\mathrm{d}s}{\mathrm{d}\varsigma}\right) = \begin{cases} \theta, & 0 < \xi < \infty,\ \eta = 0, \\ \theta - \pi/2, & \xi = 0,\ 0 < \eta < \infty. \end{cases} \tag{2.8}$$

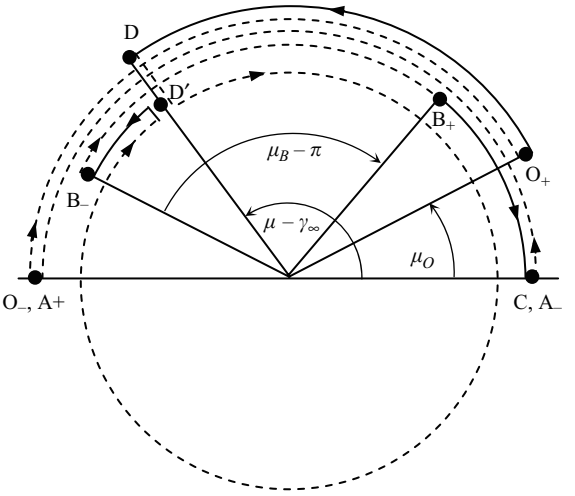

FIGURE 2. The variation of the function $\theta = \tan^{-1}(v_n/v_\tau)$ along the boundary of the fluid region. Continuous changes are shown by solid lines, step changes by dashed lines.

Then the problem is to find a function $\mathrm{d}w/\mathrm{d}\varsigma$ which satisfies the given boundary conditions (2.8). The formula

$$\frac{\mathrm{d}w}{\mathrm{d}\varsigma} = K \exp\left[-\frac{1}{\pi}\int_0^\infty \frac{\mathrm{d}\vartheta}{\mathrm{d}\xi'}\ln(\varsigma^2 - \xi'^2)\,\mathrm{d}\xi' + \frac{1}{\pi}\int_0^\infty \frac{\mathrm{d}\vartheta}{\mathrm{d}\eta'}\ln(\varsigma^2 + \eta'^2)\,\mathrm{d}\eta' + \mathrm{i}\vartheta(\infty)\right], \tag{2.9}$$

provides a solution of this boundary-value problem in the first quadrant of the complex plane ς. Here, K is an arbitrary real factor, which will be determined in the following. It can be easily verified that for $\varsigma = \xi$ or $\varsigma = \mathrm{i}\eta$ the argument of the function $\mathrm{d}w/\mathrm{d}\varsigma$ is the function $\vartheta(\varsigma)$, i.e. the boundary condition (2.8) is satisfied.

Now we have to determine the function $\theta(\varsigma)$ along the whole fluid boundary, that is, along the real and imaginary axes of the parameter region. On moving along the free surface from point O to point D, the function $\theta(\varsigma)$ increases from the value μ_O at $\varsigma = 0$ to the value $\pi - \gamma_\infty$ corresponding to the velocity direction at infinity (the point at $\varsigma = \mathrm{i}$). In order to find the left-hand side of the free surface away from the plate, we have to move along a closed line of large radius to provide the constant velocity direction. Thus, on going around an infinitesimal semicircle centred at the point $\varsigma = \mathrm{i}$ corresponding to the large radius in the physical plane, the function $\theta(\varsigma)$ changes by $\Delta\theta_D = -2\pi$. The continuous changes of the function $\theta(\varsigma)$ are shown in figure 2 by solid lines while its step changes are shown by dashed lines. Further, the function $\theta(\varsigma)$ changes continuously when moving along the free surface from point D′ to point B. At point B ($\varsigma = \mathrm{i}b$) the function $\theta(\varsigma)$ undergoes a jump equal of $\Delta\theta_B = \mu_B - \pi$ corresponding to the corner point of angle μ_B on the free surface. It is shown in figure 2 by the dashed line from point B_- to point B_+. From point B_+ to point C the normal velocity component decreases and becomes equal to zero at the leading edge of the plate, i.e. $\theta(\varsigma) \to 0$ when $\eta \to \infty$, $\xi = 0$. In the region $a < \xi < \infty$, $\eta = 0$ corresponding to the fixed plate the function $\theta(\varsigma) \equiv 0$ since $v_n = 0$ and $v_s > 0$. In the region $0 < \xi < a$, $\eta = 0$ the function $\theta(\varsigma) \equiv \pi$ since $v_n = 0$ and $v_s < 0$, thus at the point $\varsigma = a$ the function $\theta(\varsigma)$ has a jump $\Delta\theta_A = -\pi$. The final jump $\Delta\theta_O = \mu_O - \pi$ occurs at point O when moving in the vicinity of the point $\varsigma = 0$ from the plate

surface, $\xi > 0, \eta = 0$, to the free surface, $\xi = 0, \eta > 0$. By introducing the continuous function $\lambda(\varsigma)$ we can write the function $\theta(\varsigma)$ as follows

$$\theta(\varsigma) = \begin{cases} \lambda(\varsigma), & \xi = 0, \quad 0 < \eta < 1, \\ \lambda(\varsigma) + \Delta\theta_D, & \xi = 0, \quad 1 < \eta < b, \\ \lambda(\varsigma) + \Delta\theta_D + \Delta\theta_B, & \xi = 0, \quad b < \eta < \infty, \\ \lambda(\varsigma) + \Delta\theta_D + \Delta\theta_B, & a < \xi < \infty, \quad \eta = 0, \\ \lambda(\varsigma) + \Delta\theta_D + \Delta\theta_B + \Delta\theta_A, & 0 < \xi < a, \quad \eta = 0, \\ \lambda(\varsigma) + \Delta\theta_D + \Delta\theta_B + \Delta\theta_A + \Delta\theta_O, & \xi = 0, \quad \eta = 0. \end{cases} \tag{2.10}$$

where $\Delta\theta_D = -2\pi$, $\Delta\theta_B = \mu_B - \pi$, $\Delta\theta_A = -\pi$, $\Delta\theta_O = \mu_O - \pi$.

By substituting equations (2.8) and (2.10) into the first integral in (2.9), when ς varies along the real axis, and into the second integral, when ς varies along the imaginary axis of the parameter region, and evaluating the integrals over each step change of the function $\theta(\varsigma)$, we finally obtain an expression for the derivative of the complex potential in the ς-plane as

$$\frac{\mathrm{d}w}{\mathrm{d}\varsigma} = K\varsigma^{2\mu_O/\pi-1} \frac{(\varsigma^2 - a^2)}{(\varsigma^2+1)^2(\varsigma^2+b^2)^{1-\mu_B/\pi}} \exp\left[\frac{1}{\pi}\int_0^\infty \frac{\mathrm{d}\lambda}{\mathrm{d}\eta'} \ln(\varsigma^2 + \eta'^2)\, \mathrm{d}\eta'\right]. \tag{2.11}$$

The evaluation of the integrals over the step changes is done, for example, at point D ($\varsigma = \mathrm{i}$) as follows

$$\lim_{\epsilon\to 0}\int_{1-\epsilon}^{1+\epsilon} \frac{\mathrm{d}\theta}{\mathrm{d}\eta'} \ln(\varsigma^2 + \eta'^2)\, \mathrm{d}\eta' = \ln(1+\varsigma^2) \lim_{\epsilon\to 0}\int_{1-\epsilon}^{1+\epsilon} \frac{\mathrm{d}\theta}{\mathrm{d}\eta'}\, \mathrm{d}\eta' = \Delta\theta_D \ln(1+\varsigma^2).$$

Integration of equation (2.11) in the parameter region allows us to obtain the function that conformally maps the parameter region onto the corresponding region in the complex potential plane:

$$w(\varsigma) = w(0) + K\int_0^\varsigma \frac{\varsigma^{2\mu_O/\pi-1}(\varsigma^2 - a^2)}{(\varsigma^2+1)^2(\varsigma^2+b^2)^{1-\mu_B/\pi}} \exp\left[\frac{1}{\pi}\int_0^\infty \frac{\mathrm{d}\lambda}{\mathrm{d}\eta'} \ln(\eta'^2 + \varsigma^2)\mathrm{d}\eta'\right] \mathrm{d}\varsigma. \tag{2.12}$$

Dividing (2.11) by (2.6), we derive the expression

$$\frac{\mathrm{d}z}{\mathrm{d}\varsigma} = \frac{\mathrm{d}w/\mathrm{d}\varsigma}{\mathrm{d}w/\mathrm{d}z} = K\varsigma^{2\mu_O/\pi-1} \frac{(\varsigma + a)^2}{(\varsigma^2+1)^2(\varsigma^2+b^2)^{1-\mu_B/\pi}} \exp\left[\frac{1}{\pi}\int_0^\infty \frac{\mathrm{d}\lambda}{\mathrm{d}\eta'} \ln(\eta'^2 + \varsigma^2)\, \mathrm{d}\eta' + \frac{\mathrm{i}}{\pi}\int_0^\infty \frac{\mathrm{d}\ln v}{\mathrm{d}\eta'} \ln\left(\frac{\mathrm{i}\eta' - \varsigma}{\mathrm{i}\eta' + \varsigma}\right) \mathrm{d}\eta' + \mathrm{i}(\pi + \beta)\right], \tag{2.13}$$

whose integration in equation (2.2) gives the function that conformally maps the first quadrant of the parameter plane onto the stationary z-plane. Integration along the imaginary axis in the parameter region provides the free surface of the flow.

The expression for the complex velocity (2.6) has no singularity at the point $\varsigma = \mathrm{i}b$. This means that the velocity changes continuously in the region $|\varsigma - \mathrm{i}b| < \varepsilon$ of the parameter plane, which corresponds to the splash jet in the physical plane. In contrast, the derivative of the flow potential (equation (2.11)) has the integrable singularity

$$\frac{\mathrm{d}w}{\mathrm{d}\varsigma} \sim (\varsigma - \mathrm{i}b)^{\mu_B/\pi - 1},$$

if $\mu_B > 0$. The same singularity occurs in the expression for the function $\mathrm{d}z/\mathrm{d}\varsigma$, whose integration in the vicinty of the point $\varsigma = \mathrm{i}b$ gives

$$z(\varsigma) - z_B = C^* \frac{\pi}{\mu_B} (\varsigma - \mathrm{i}b)^{\mu_B/\pi}$$

where C^* is a complex constant.

The functions $v(\eta)$ and $\lambda(\eta)$ are determined from the dynamic and kinematic boundary conditions in the following. The parameters a, K, μ_B, are determined from the following physical considerations.

At infinity, the complex velocity approaches the value $v_\infty \exp(-\mathrm{i}\gamma_\infty)$. By taking the argument of equation (2.6) when $\varsigma = \mathrm{i}$, we obtain the following nonlinear condition

$$\frac{1}{\pi} \int_0^\infty \frac{\mathrm{d} \ln v}{\mathrm{d}\eta'} \ln \left| \frac{\eta' - 1}{\eta' + 1} \right| \mathrm{d}\eta' + 2 \arctan \frac{1}{a} - \alpha = 0. \tag{2.14}$$

The wetted length of the flat plate grows as $V_0 t$, and then the length of the segment OC in the stationary plane is unity, that is, $|z_O| = 1$. Hence, the following condition is obtained:

$$\int_0^\infty \left| \frac{\mathrm{d}z}{\mathrm{d}\varsigma} \right|_{\varsigma=\xi} \mathrm{d}\xi = 1. \tag{2.15}$$

Finally, an additional condition is obtained by requiring that the y-coordinate of the free surface at infinity on the right and on the left be the same, that is

$$\mathrm{Im}\left(\oint_{\varsigma=\mathrm{i}} \frac{\mathrm{d}z}{\mathrm{d}\varsigma} \mathrm{d}\varsigma \right) = \mathrm{Im}\left(\pi \mathrm{i} \operatorname*{Res}_{\varsigma=i} \frac{\mathrm{d}z}{\mathrm{d}\varsigma} \right) = \mathrm{Im}\left(\pi \mathrm{i} \lim_{\varsigma=i} \frac{\mathrm{d}}{\mathrm{d}\varsigma} \left(\frac{\mathrm{d}z}{\mathrm{d}\varsigma} (\varsigma - \mathrm{i})^2 \right) \right) = 0.$$

By evaluating the integral using the theorem of residues, we find

$$-\frac{1}{\pi} \int_0^\infty \frac{\mathrm{d}\lambda}{\mathrm{d}\eta'} \frac{\mathrm{d}\eta'}{\eta'^2 - 1} + \frac{1}{a^2 + 1} + \frac{1 - \mu_B/\pi}{b^2 - 1} + \frac{\mu_O}{\pi} - 1 = 0. \tag{2.16}$$

2.2. *Dynamic and kinematic boundary conditions*

Along the free surface the pressure is constant and equal to the atmospheric pressure P_a. The Cauchy–Lagrange integral written in the physical plane for point O and an arbitrary point in the flow gives

$$\left. \frac{\partial \Phi}{\partial t} \right|_Z + \frac{V^2}{2} + \frac{P}{\rho} = \left. \frac{\partial \Phi}{\partial t} \right|_{Z=0} + \frac{V_0^2}{2} + \frac{P_a}{\rho}, \tag{2.17}$$

By taking advantage of the flow self-similarity alone, the Cauchy–Lagrange integral can be reduced to a differential equation relating the derivatives of the velocity modulus and angle with the free surface, obtained by Semenov & Iafrati (2006)

$$\frac{\mathrm{d} \ln v}{\mathrm{d}s} = \frac{s \sin\theta}{v + s \cos\theta} \frac{\mathrm{d}\theta}{\mathrm{d}s}. \tag{2.18}$$

By multiplying both sides of equation (2.18) by $\mathrm{d}s/\mathrm{d}\eta$ and taking into account that $\mathrm{d}\theta/\mathrm{d}s = \mathrm{d}\lambda/\mathrm{d}s$, $0 < \eta < 1$, we obtain the following integro-differential equation:

$$\frac{\mathrm{d} \ln v}{\mathrm{d}\eta} = \frac{s \sin\theta}{v + s \cos\theta} \frac{\mathrm{d}\lambda}{\mathrm{d}\eta} \tag{2.19}$$

where

$$s(\eta) = -\int_0^\eta \left|\frac{\mathrm{d}z}{\mathrm{d}u}\right|_{u=i\eta} \mathrm{d}\eta = -K\int_0^\eta \frac{\eta^{2\mu_O/\pi-1}}{v(\eta)} \frac{\eta^2+a^2}{(1-\eta^2)^2|b^2-\eta^2|^{1-\mu_B/\pi}} \times \exp\left[\frac{1}{\pi}\int_0^\infty \frac{\mathrm{d}\lambda}{\mathrm{d}\eta'} \ln|\eta'^2-\eta^2|\mathrm{d}\eta'\right]\mathrm{d}\eta. \quad (2.20)$$

Equations (2.18)–(2.20) hold only along the right-hand side. The same equations can be obtained for the segments DB and BC, but the coordinate s should be taken starting from point B, at which the potential should be $W(Z_B, t) = 0$ (Shorygin 1995).

The kinematic boundary condition expresses the fact that the free surface is a material surface which is made up of the same liquid particles. From the general equation of classical hydrodynamics

$$\frac{\mathrm{d}\boldsymbol{U}}{\mathrm{d}t} = -\frac{1}{\rho}\mathrm{grad}\,P,$$

where ρ is the liquid density, applied to the particles on the free surface where the pressure $P = P_a$ is a constant, it follows that the acceleration of the liquid particles, $\mathrm{d}\boldsymbol{U}/\mathrm{d}t$, is orthogonal to the free surface

$$Re\left(\frac{\mathrm{d}\boldsymbol{U}}{\mathrm{d}t}\overline{\mathrm{d}Z}\right) = 0. \quad (2.21)$$

Here, $\mathrm{d}Z$ is a small element along the free boundary. Let γ denote the argument of the velocity vector $\boldsymbol{U}$ and $\delta = \gamma + \theta$ the argument of the element $\mathrm{d}Z$. By using similarity relations to pass from the variables in the physical plane to the corresponding ones in the stationary plane, the condition (2.21) leads to a differential equation relating the derivatives of the modulus and angle of the velocity vector. Equation (2.21) takes the form

$$\frac{\mathrm{d}\gamma}{\mathrm{d}\eta} = -\frac{1}{\tan\theta}\frac{\mathrm{d}\ln v}{\mathrm{d}\eta}. \quad (2.22)$$

By writing equation (2.6) for $\varsigma = i\eta$, another equation for γ can be obtained as

$$\gamma = \mathrm{Im}\left(\ln\overline{\frac{\mathrm{d}w}{\mathrm{d}z}}\right),$$

and its differentiation with respect to η yields

$$\frac{\mathrm{d}\gamma}{\mathrm{d}\eta} = \frac{2a}{a^2+\eta^2} - \frac{1}{\pi}\int_0^\infty \frac{\mathrm{d}\ln v}{\mathrm{d}\eta'}\frac{2\eta'}{\eta'^2-\eta^2}\mathrm{d}\eta'. \quad (2.23)$$

From equations (2.22) and (2.23), the following integral equation in $\mathrm{d}\ln v/\mathrm{d}\eta$ is obtained:

$$-\frac{1}{2\tan\theta}\frac{\mathrm{d}\ln v}{\mathrm{d}\eta} + \frac{1}{\pi}\int_0^\infty \frac{\mathrm{d}\ln v}{\mathrm{d}\eta'}\frac{\eta'}{\eta'^2-\eta^2}\mathrm{d}\eta' = \frac{a}{a^2+\eta^2}. \quad (2.24)$$

The system of equations (2.14)–(2.16), (2.19) and (2.24) allows us to determine the parameters a, μ_B, K and the functions $v(\eta)$, $\lambda(\eta)$ together with the function $\theta(\eta)$ related to $\lambda(\eta)$ by equation (2.10). Once the functions $v(\eta)$ and $\theta(\eta)$ are evaluated, the velocity modulus at the leading edge of the plate, v_C, and the contact angle between the plate and the free surface are determined as follows:

$$v_C = \lim_{\eta\to\infty} v(\eta), \quad \mu_O = \lim_{\eta\to 0}\theta(\eta). \quad (2.25)$$

The last unknown parameter b is determined so that the dynamic boundary condition (2.17) at the leading edge of the plate is satisfied. Applying this equation to points O and C and using self-similar variables, the following equation is obtained:

$$v_C^2 = -1 - 2\phi_C, \tag{2.26}$$

where $\phi_C = Re\,[w(\varsigma)]|_{\varsigma=\xi\to\infty}$ is determined from equation (2.12).

The pressure coefficient $p = 2P/\rho V_\infty^2$ along the plate is determined from equation (2.17) assuming the similarity of the pressure distribution in time. This means that the pressure is the same in time at the points $S = V_0 t s$ in the physical plane

$$Z(S,t) = V_0 t\left(1 - \frac{S}{V_0 t}\right)\mathrm{e}^{\mathrm{i}\beta}, \quad 0 \leqslant S \leqslant V_0 t. \tag{2.27}$$

Determining the term $\partial\Phi/\partial t$ in equation (2.17) with the use of self-similar variables and equation (2.27) and taking into account that the imaginary part of the complex potential equals zero on the solid surface, the following expression for the pressure coefficient is obtained (Semenov & Iafrati 2006):

$$p(\xi) = -\frac{2(\phi + sv) + (1-v)^2}{v_\infty^2}, \quad 0 \leqslant \xi \leqslant \infty \tag{2.28}$$

where ϕ, v, s are determined from equations (2.12), (2.6) and (2.13) as follows:

$$\phi = Re\,[w(\varsigma)]|_{\varsigma=\xi}, \quad v = \left|\frac{\mathrm{d}w}{\mathrm{d}z}\right|_{\varsigma=\xi}, \quad s(\xi) = \int_0^\xi \left|\frac{\mathrm{d}z}{\mathrm{d}\varsigma}\right|_{\varsigma=\xi}\mathrm{d}\xi, \quad v_\infty = v(\eta)|_{\eta=1}.$$

By integrating the pressure coefficient along the plate, the following expression for the normal force coefficient is obtained:

$$C_n = \frac{1}{0.5\rho V_\infty^2 H}\int_0^{V_0 t} P(S)\mathrm{d}S = \frac{1}{v_\infty h}\int_0^\infty p(\xi)\frac{\mathrm{d}s}{\mathrm{d}\xi}\mathrm{d}\xi \tag{2.29}$$

where $H = V_\infty t h$, $h = \sin\gamma_\infty/\tan(\gamma_\infty - \alpha) - \cos\gamma_\infty$, is the distance between the point where the leading edge of the flat plate touches the free surface and the current intersection point of the undisturbed free surface and the flat plate, which is chosen as the characteristic length.

The pressure is characterized by a jump in its derivative about the stagnation point, which is related to the behaviour of the velocity modulus. Differentiating the dependence (2.28) along the spatial coordinate s, we obtain

$$\frac{\mathrm{d}p}{\mathrm{d}s} = -\frac{2}{v_\infty^2}\left(\frac{\mathrm{d}\phi}{\mathrm{d}s} + (s - 1 + v)\frac{\mathrm{d}v}{\mathrm{d}s} + v\right). \tag{2.30}$$

At the stagnation point both the velocity modulus and the tangential derivative of the velocity potential vanish, i.e. $v = 0$ and $\mathrm{d}\phi/\mathrm{d}s = v_s = 0$. Analysing the behaviour of the derivatives $\mathrm{d}v/\mathrm{d}\xi$ using equation (2.6) and $\mathrm{d}s/\mathrm{d}\xi = |\mathrm{d}z/\mathrm{d}\varsigma|_{\varsigma=\xi}$ in equation (2.13) shows that about the stagnation point $\xi = a$ the quantity $\mathrm{d}v/\mathrm{d}s = (\mathrm{d}v/\mathrm{d}\xi)/(\mathrm{d}s/\mathrm{d}\xi)$ is finite and different from zero, and its sign changes about the stagnation point. As follows from equation (2.30), the sign of $\mathrm{d}p/\mathrm{d}s$ at the stagnation point $s_A < 1$ also changes, which leads to a cusp point in the pressure distribution along the plate. Since for steady flows $\mathrm{d}p/\mathrm{d}s = 0$ at the stagnation point, this effect occurs due to the flow unsteadiness.

2.3. *Asymptotic behaviour of the free surface.*

The physical model of the flow under consideration assumes that at time $t=0$ the flow region occupies the half-space with the initial free-surface shape $y(x,0)=0$, $-\infty<x<\infty$. For any time $t>0$ the perturbations of the free-surface caused by the entry of the flat plate decay at infinity, and therefore the free-surface level at infinity remains zero, i.e. $y_\infty=y(\pm\infty,t)=0$ (Howison *et al.* 2004). The same considerations for steady flows with free boundaries that expand without limit do not lead to the same conclusion because even small perturbations of the velocity at infinity may lead to an infinite change of the free surface during infinite time. Examples of such flows as well as their classic solutions are well known, such as, jet flows past bodies or flows past bodies planing over the free surface. The classic solutions of these problems without gravity predict an infinite level of the free surface at infinity $y_\infty\sim\log|x|$, $x\to\pm\infty$, which is known as Green's paradox (Green 1935). Let us check our solution for the behaviour of the coordinate of the free surface at infinity.

For $\varsigma=\mathrm{i}\eta$, which corresponds to the free surface, equation (2.13) can be written as follows:

$$\left.\frac{\mathrm{d}z}{\mathrm{d}\varsigma}\right|_{\varsigma=\mathrm{i}\eta}=\frac{\mathrm{d}s}{\mathrm{d}\eta}\mathrm{e}^{\mathrm{i}\delta}$$

where s is the spatial coordinate along the free surface and δ is the argument of the element $\mathrm{d}z$ determined from equation (2.13)

$$\delta(\eta)=\lambda(\eta)+2\arctan\frac{\eta}{a}+\frac{1}{\pi}\int_0^\infty\frac{\mathrm{d}\ln v}{\mathrm{d}\eta'}\ln\left|\frac{\eta'-\eta}{\eta'+\eta}\right|\mathrm{d}\eta'+\gamma_\infty-\alpha-\pi. \tag{2.31}$$

At the point $\eta=1$ the function $\mathrm{d}s/\mathrm{d}\eta$ has the singularity $(1-\eta)^{-2}$. Also, when $\eta\to1$, $\delta\to0$ and $x\to\infty$ to give $\mathrm{d}x/\mathrm{d}\eta\approx\mathrm{d}s/\mathrm{d}\eta$ and $\mathrm{d}y/\mathrm{d}\eta\approx\delta\,\mathrm{d}s/\mathrm{d}\eta$. In order to estimate the leading order of the function $\delta(\eta)$ near the point $\eta=1$, consider the expansion

$$\delta(\eta)=\delta(1)+\left.\frac{\mathrm{d}\delta}{\mathrm{d}\eta}\right|_{\eta=1}(\eta-1)+O(\eta-1)^2.$$

Setting $\eta=1$ in equation (2.31) and taking into account that $\lambda(1)=\pi-\gamma_\infty$, we obtain the same equations as (2.14), i.e. $\delta(1)=0$.

Differentiating equation (2.31)

$$\frac{\mathrm{d}\delta}{\mathrm{d}\eta}=\frac{\mathrm{d}\lambda}{\mathrm{d}\eta}+\frac{2a}{a^2+\eta^2}-\frac{2}{\pi}\int_0^\infty\frac{\mathrm{d}\ln v}{\mathrm{d}\eta'}\frac{\eta'\mathrm{d}\eta'}{\eta'^2-\eta^2}.$$

and substituting

$$\frac{\mathrm{d}\lambda}{\mathrm{d}\eta}=\frac{1}{\tan\theta}\frac{\mathrm{d}\ln v}{\mathrm{d}\eta}$$

obtained from the dynamic boundary condition (2.23) when $\eta\to1$ and thus $s\to\infty$, we have

$$\left.\frac{\mathrm{d}\delta}{\mathrm{d}\eta}\right|_{\eta=1}=\frac{1}{\tan\theta}\frac{\mathrm{d}\ln v}{\mathrm{d}\eta}+\frac{2a}{a^2+1}-\frac{2}{\pi}\int_0^\infty\frac{\mathrm{d}\ln v}{\mathrm{d}\eta'}\frac{\eta'\mathrm{d}\eta'}{\eta'^2-1}. \tag{2.32}$$

This expression is equal to zero in view of the integral equation (2.24) at the point $\eta=1$, which is obtained from the kinematic boundary condition. Thus the function $\delta(\eta)\sim O(\eta-1)^2$, and the integral of the function $\mathrm{d}y/\mathrm{d}\eta\approx\delta\,\mathrm{d}s/\mathrm{d}\eta$ has a finite value.

Steady flows usually have a stagnation point similar to point A. Also, the normal component of the velocity on the free boundaries equals zero, i.e. the functions

$\lambda(\eta) = \theta(\eta) \equiv 0$. The velocity modulus along the free boundaries is also constant, i.e. $\mathrm{d}\ln v/\mathrm{d}\eta \equiv 0$. For this case from equation (2.32) it follows that $\mathrm{d}\delta/\mathrm{d}\eta \neq 0$. This means that due to the stagnation point the expressions $\mathrm{d}y/\mathrm{d}\eta = \delta\,\mathrm{d}s/\mathrm{d}\eta \sim (\eta-1)^{-1}$ and $\mathrm{d}x/\mathrm{d}\eta = \mathrm{d}s/\mathrm{d}\eta \sim (\eta-1)^{-2}$ have a first- and second-order singularity, respectively. Thus the function $y(x)$ has a logarithmic singularity, $y \sim \log|x|$, which corresponds to Green's paradox.

The present solution predicts the increase of the free-surface elevation as $Y(x,t) = y(x)t$, where $y(x) \to 0$, $x \to \pm\infty$, from the self-similar statement of the problem, which is valid at initial stages of water entry. The next time-dependent stage of complete entry is an intermediate stage between the initial stage and the final stage of the corresponding steady flow for which $y \sim \log|x|$ at infinity. Thus, for time-dependent problems, the logarithmic singularity $y \sim \log|x|$ in the shape of the free surface appears locally near the body and extends to infinity as $t \to \infty$. This has also been shown by Needham, Billingham & King (2007), who studied the time-dependent flow caused by the impulsive motion of a rigid vertical plate using the method of matched asymptotic expansions.

3. Numerical method

3.1. *Numerical approach*

The method of successive approximations is applied to solve the system of nonlinear equations including the integro-differential equation (2.19) and the integral equation (2.24) containing a Cauchy-type kernel. The method consists of applying the Hilbert transform to solve equation (2.24) and determining the $(k+1)$th approximation as follows

$$\left(\frac{\mathrm{d}\ln v}{\mathrm{d}\eta}\right)^{(k+1)} = \frac{4}{\pi}\int_0^\infty \left\{\frac{1}{2\tan\theta}\frac{\mathrm{d}\ln v}{\mathrm{d}\eta'} + \frac{a}{a^2+\eta'^2}\right\}^k \frac{\eta'}{\eta'^2-\eta^2}\mathrm{d}\eta'. \tag{3.1}$$

From equation (2.19) the $(k+1)$th approximation of the derivative $\mathrm{d}\lambda/\mathrm{d}\eta$ is obtained

$$\left(\frac{\mathrm{d}\lambda}{\mathrm{d}\eta}\right)^{k+1} = \frac{v^{k+1} + s^k\cos\theta^k}{s^k\sin\theta^k}\left(\frac{\mathrm{d}\ln v}{\mathrm{d}\eta}\right)^{k+1} \tag{3.2}$$

where

$$\theta(\eta) = \begin{cases} \lambda(\eta), & 0 < \eta < b \\ \lambda(\eta) + \pi - \mu_B, & b < \eta < \infty, \end{cases}$$

the integration of which along the imaginary axis of the parameter region provides the $(k+1)$th approximation for the function $\theta(\eta)$. The system of nonlinear equations (2.14)–(2.16) is solved at each iteration. The iteration procedure is repeated for each value of the parameter b when solving equation (2.26) for the parameter b. The functions $v(\eta)$ and $\theta(\eta)$ have two singularities at points O and B as follows from equations (3.1) and (3.2). At these points the flow potential and the arclength coordinate were set equal to zero to derive these integral equations. On the other hand, the functions $v(\eta)$ and $\theta(\eta)$ are bounded by their definition. In order to evaluate the integral in equation (3.1), the lower limit in the integral is set equal to a small value ε as discussed in the following.

In discrete form, the solution is sought on a set of points η_j, $j = 1 \ldots 3N$ lying on the intervals: $0 < \eta_j < 1$, $j = 1 \ldots N$; $1 < \eta_j \leqslant b$, $j = N+1 \ldots 2N$; $b < \eta_j \leqslant \eta_{3N}$, which correspond to the segments OD, DB and BC, respectively. The points $0 < \eta_j < 1$ are fixed while the points on the other intervals depend on the parameter b and

	μ_O/π			μ_B/π		
$\eta_1, \eta_{2N+1} - b$	$N = 50$	$N = 100$	$N = 200$	$N = 50$	$N = 100$	$N = 200$
10^{-5}	0.03476	0.03469	0.03461	0.31659	0.31733	0.31758
10^{-6}	0.03465	0.03460	0.03455	0.30726	0.30812	0.30838
10^{-7}	0.03461	0.03458	0.03457	0.30303	0.30422	0.30450
10^{-8}	0.03458	0.03457	0.03457	0.30094	0.30257	0.30286
10^{-9}	0.03456	0.03456	0.03457	0.29965	0.30145	0.30211
10^{-10}	0.03453	0.03455	0.03457	0.29872	0.30124	0.30207

TABLE 1. Tip jet angles at the contact point O and at point B on the free surface for vertical flat-plate water entry with angle of incidence $\alpha = 30°$. The results in the columns correspond to different distances between the singular point $\eta = 0$ ($\eta = b$) and the nearest node. The results in the rows correspond to different numbers of nodes.

are distributed as a geometric series with higher density near the singular points $\eta_0 = 0$, $\eta_{2N} = b$. The functions $v(\eta)$ and $\theta(\eta)$ are interpolated linearly on the intervals (η_{j-1}, η_j) to obtain analytical expressions for the integrals in (2.6) and (2.11), thus reducing the computational effort.

The arclengths s_1, s_{2N-1}, s_{2N+1} nearest to points O and B are evaluated analytically taking into account the singularity in the integrand in equation (2.20), thus yielding

$$\left.\begin{aligned} s_1 &= -K\frac{a^2}{b^{1-\mu_B/\pi}}\exp\left(\frac{2}{\pi}\int_0^\infty \frac{\mathrm{d}\lambda}{\mathrm{d}\eta'}\ln\eta'\mathrm{d}\eta'\right)\frac{\pi\eta_1^{2\mu_O/\pi}}{2\mu_O}, \\ s_{2N+1} &= \frac{K}{2v_B}b^{2\mu_O/\pi-1}\frac{(a^2+b^2)}{(1-b^2)^2}\exp\left(\frac{1}{\pi}\int_0^\infty \frac{\mathrm{d}\lambda}{\mathrm{d}\eta'}\ln|\eta'^2-b^2|\mathrm{d}\eta'\right)\frac{\pi(\eta_{2N+1}-b)^{\mu_B/\pi}}{\mu_B}, \end{aligned}\right\} \tag{3.3}$$

where $v_B = v(\eta)|_{\eta=b}$. Since the distances of points η_{2N-1}, η_{2N+1} from point $\eta_{2N} = b$ are chosen to be the same, i.e. $\eta_{2N+1} - b = b - \eta_{2N-1}$, then $s_{2N-1} = -s_{2N+1}$.

3.2. *Validation of the numerical approach*

To evaluate the accuracy and mesh-independence of the results, several distributions of nodes with different values of the smallest intervals near the singular points $\eta = 0$ and $\eta = b$ and different numbers of nodes have been employed. Table 1 gives the tip jet angles μ_O/π and μ_B/π predicted for the vertical flat-plate water entry with angle of incidence $\alpha = 30°$. The columns show the results for the smallest interval in the node distribution $\Delta = \eta_1 = b - \eta_{2N-1} = \eta_{2N+1} - b$ varying through the range $10^{-10} - 10^{-5}$ for a fixed number of nodes. The rows show the results for number of nodes $N = 50,\ 100$ and 200 at fixed location of points $\eta_1,\ \eta_{2N-1}$ and η_{2N+1}.

The solution converges when both the number $N \to \infty$ and the smallest interval $\Delta \to 0$. At a fixed Δ, the accuracy is increased with increasing N. On other hand, at a fixed N there exists an optimum value Δ^* such that a reasonable accuracy is obtained both for the numerical integration along the imaginary axis of the parameter plane and for the computation of the derivatives $\mathrm{d}\ln v/\mathrm{d}\eta$ and $\mathrm{d}\lambda/\mathrm{d}\eta$ near the singular points. The node distribution geometry is such that for too small values of Δ the node density becomes higher near the singular points and lower for the rest of the corresponding interval, which may decrease the integration accuracy. As can be seen from table 1, the values $\mu_O/\pi = 0.03457$ and $\mu_B/\pi = 0.30207$ obtained for $N = 200$ and $\Delta = 10^{-10}$ can be obtained for $N = 50$ and a value of Δ lying in the range from 10^{-8} to 10^{-7}.

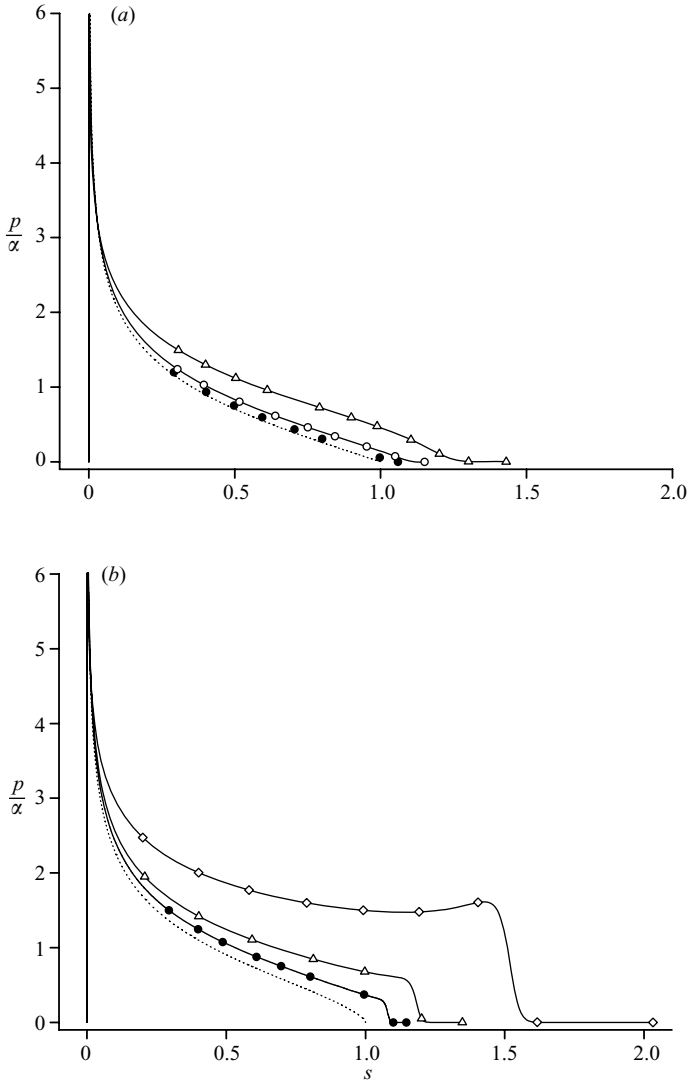

FIGURE 3. Pressure coefficient, divided by α, along the plate entering the free surface (*a*) vertically and (*b*) obliquely $\gamma_\infty = 45°$. The results for the present nonlinear solution (solid lines, •, $\alpha = 1°$; ○, $\alpha = 2°$; △, $\alpha = 3°$; ◇, $\alpha = 10°$) are compared with Wang's linear solution (dotted line).

In the theoretical framework, the contact angle is an important parameter because it influences the spatial arclength coordinate starting at the contact point. If we are able to obtain a good accuracy for the contact angle, then we can be sure that the accuracy for the other parameters is good too. In contrast, in the case of a poor accuracy for the contact angle, the adequacy of the accuracy for the other flow parameters should be studied numerically.

For validation, the results predicted by the present nonlinear theory are compared with those predicted by Wang's (1977, 1979) linear theory. In figure 3, a comparison is made between the calculated pressure coefficient divided by the angle of attack α along a plate entering the water (*a*) vertically and (*b*) obliquely and that predicted

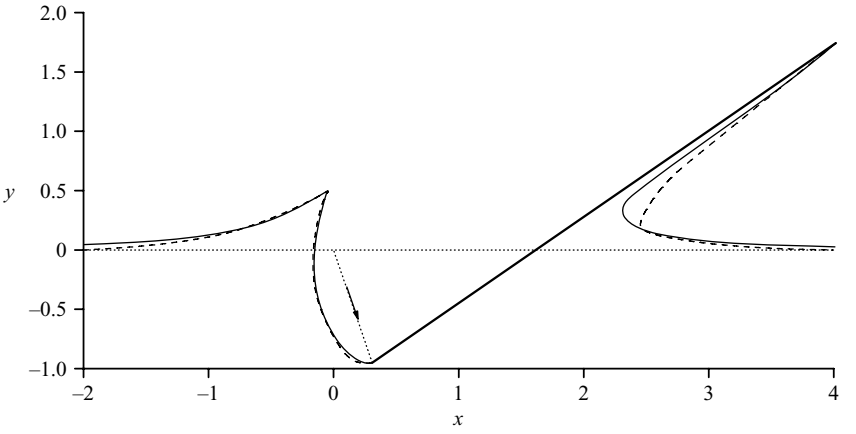

FIGURE 4. The free surface shape for the case of the oblique water entry of a flat plate at $\gamma_\infty = 108^\circ$ and $\alpha = 72^\circ$. The present results (solid lines) are compared with Chekin's (1989) nonlinear theory (dashed lines).

by Wang's linear theory. Within the framework of the linear theory, the pressure coefficient divided by the angle of attack is the same for various angles of attack. It is not the same for the nonlinear theory. The difference between the dotted and solid lines shows nonlinear effects in the water entry flow. As expected, with decreasing angle of attack the results approach those predicted by the linear theory, which confirms the validity of the method presented and its numerical realization. For oblique water entry at the same angle of attack, the effects of nonlinearity increase as a comparison between figures 3(*a*) and 3(*b*) shows. This is due to the fact that small deadrise angles cause the slamming effect studied in detail for the water entry of symmetric wedges, in particular, by Zhao & Faltinsen (1993).

In figure 4, the free-surface shape obtained for oblique water entry of a flat plate at $\gamma_\infty = 108^\circ$ and $\alpha = 72^\circ$ is shown and compared with the corresponding result of Chekin's (1989) nonlinear theory. Agreement between the two results is good. The differences may be due to the quality of drawing in Chekin's paper since the normal force coefficient $C_n = 9.32$ obtained is also close to the value $C_n = 9.28$ presented in that paper. Note that the x-coordinate of the splash jet relative to the point at which the leading edge of the plate touches the free surface is about zero. The same property will be seen later for other initial conditions.

4. Numerical results

4.1. *Vertical water entry of a flat plate*

Table 2 shows the predicted angles and elevations of the free boundary at the contact point (point O) and at the tip of the splash (point B), the pressure at the stagnation point and the normal force coefficient. The elevation of the free boundary at the intersection point is higher than at the tip of the splash jet on the free surface for $\alpha < 80^\circ$. For $\alpha = 85^\circ$, the splash jet elevation becomes higher, and it rises rapidly.

Table 2 also gives the contact angles predicted by Zhao & Faltinsen (1993) for the symmetric entry of a wedge with a half-angle equal to the deadrise angle β for the flat plate. As can be seen from the table, the contact angle for the flat plate is only slightly smaller than for the symmetric wedge entry. This means that the flow

α	β	μ_O/π (ZF)	μ_O/π	μ_B/π	y_O	y_B	p_A	C_n
3	87	—	0.0880	0.456	0.149	0.021	1.03	1.07
5	85	—	0.0816	0.432	0.228	0.025	1.06	1.15
9	81	0.0715	0.0707	0.400	0.374	0.047	1.12	1.34
20	70	0.0499	0.0487	0.334	0.733	0.115	1.31	1.90
30	60	0.0359	0.0345	0.302	1.024	0.194	1.55	2.57
40	50	0.0251	0.0237	0.278	1.275	0.282	1.87	3.48
50	40	0.0166	0.0154	0.258	1.480	0.392	2.34	4.77
60	30	0.00991	0.0089	0.234	1.627	0.542	3.11	6.78
70	20	0.00478	0.0041	0.216	1.717	0.772	4.44	10.5
80	10	0.00134	0.0011	0.196	1.725	1.253	8.86	20.8
85	5	—	0.0003	0.177	1.619	1.880	19.4	40.2

TABLE 2. Main reference parameters for vertical $\gamma_\infty = 90^\circ$ flat-plate water entry with several angles of attack α. ZF denotes results from Zhao & Faltinsen.

boundary conditions far from the tip jet have little effect on the contact angle and thus on the slamming pressure peak that occurs at small deadrise angles.

In figure 5, streamline patterns are shown for three angles of attack that correspond to deadrise angles of 70°, 45° and 5°. The figure clearly shows the location of the stagnation point and the formation of a splash jet on the free surface. The location of the contact point of the free surface and the flat plate corresponds to the trailing edge of the plate shown in figures 5(*a*) and 5(*b*), but for case (*c*) this point is outside the plotted field. Note that the x-coordinate of the tip of the splash is about equal to the x-coordinate of the point at which the leading edge of the plate touched the free surface at initial time $t = 0$ for all the cases considered. Therefore, at the tip of the splash jet the x-component of the velocity relative to this point is zero. The extrapolation of these results leads to the conjecture that this is also true for smaller deadrise angles.

The pressure distributions along a plate vertically entering the free surface are shown in figure 6 for several deadrise angles. For larger deadrise angles the location of the stagnation point is closer to the leading edge where the pressure gradient $\mathrm{d}p/\mathrm{d}s$ is very high for deadrise angles $\beta = 60^\circ$ and 45°, thus the cusp due to the change of sign in $\mathrm{d}p/\mathrm{d}s$ discussed at the end of § 2 is invisible. It appears for a deadrise angle of 30° as a small local minimum. For this case a slamming pressure peak, which has been thoroughly studied for symmetric wedge impact (Zhao & Faltinsen 1993), also appears. Clearly, for smaller deadrise angles the unsteady components dominate in the flow parameters.

4.2. *Oblique entry*

Table 3 gives the solutions obtained for flat-plate water entry with the horizontal velocity component different from zero, which corresponds to oblique flat-plate water entry. The results are reported for $\gamma_\infty = 45^\circ$ in terms of the contact angle, the angle at the tip of the splash jet, the free boundary elevation at the intersection point and at the tip of the splash jet, the pressure at the stagnation point and the normal force coefficient. From the results it can be seen that the angle at the tip of the splash jet $\mu_B \to \gamma_\infty$ as $\alpha \to 0$. When the values of the contact angle μ_O presented in table 1 are compared with those presented in table 3, it can be seen that they are close for the same deadrise angles. This is also true for μ_B at small deadrise angles. Increasing the horizontal velocity component decreases the vertical one since they are related for

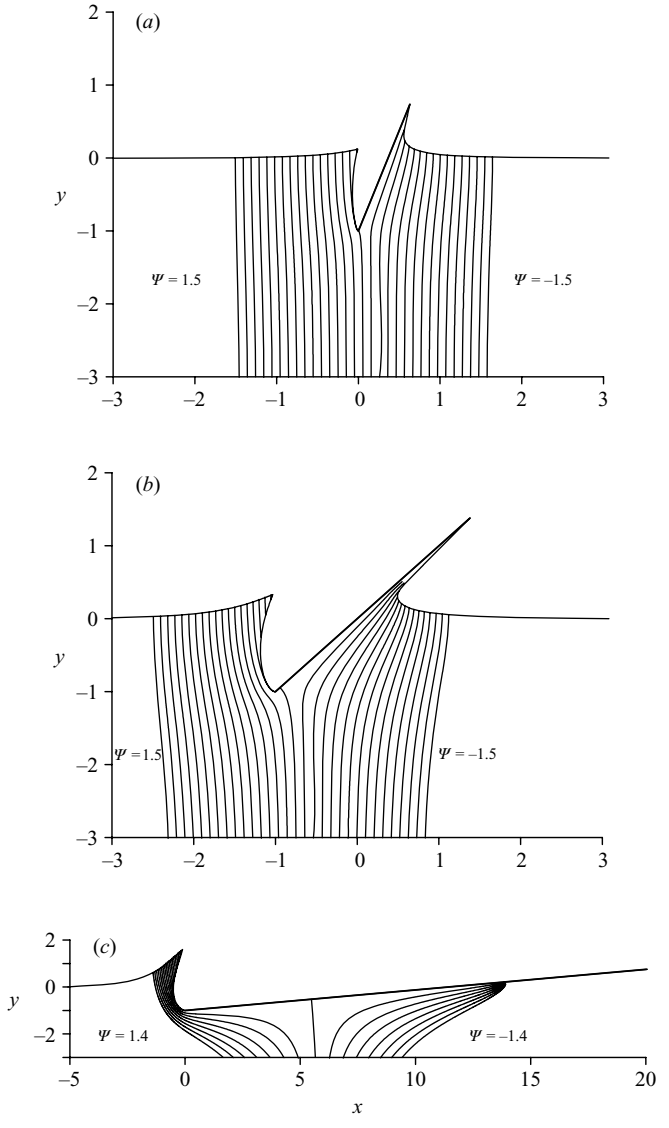

FIGURE 5. Free streamline patterns for vertical flat-plate water entry for several deadrise angles: (*a*) $\beta = 70°$; (*b*) $\beta = 45°$; (*c*) $\beta = 5°$. The interval of the streamfunction Ψ is 0.1 in (*a*, *b*) and 0.2 in (*c*).

the same magnitude of the entry velocity. As expected, from the results presented in table 2 and table 3 it follows that the lower the vertical velocity component, the lower the elevation of the free surface, the pressure at the stagnation point and the normal force coefficient.

In figure 7, streamline patterns are shown for oblique flat-plate water entry for two angles of attack of 20° and 40°, which correspond to deadrise angles of 25° and 5°, respectively. In figure 7(*a*) the trailing edge of the plate corresponds to its intersection with the free surface. As noted above for vertical entry, the x-coordinate of the tip of the splash jet does not change and corresponds to the x-coordinate where the leading edge touched the free surface, i.e. the x-velocity component at the tip of the splash jet is zero.

α	β	μ_O/π	μ_B/π	y_O	y_B	p_A	C_n
0.1	44.9	0.0316	0.250	0.018	0.001	1.00	0.68
3	42	0.0248	0.247	0.196	0.030	1.04	1.08
5	40	0.0217	0.239	0.282	0.051	1.07	1.24
9	36	0.0167	0.229	0.428	0.101	1.15	1.58
15	30	0.0110	0.215	0.615	0.190	1.31	2.21
20	25	0.0074	0.205	0.751	0.284	1.49	2.94
25	20	0.0047	0.195	0.870	0.402	1.75	3.98
30	15	0.0026	0.185	0.974	0.562	2.19	5.65
35	10	0.0012	0.174	1.057	0.800	3.08	8.83
40	5	0.0003	0.153	1.078	1.282	5.23	50.3

TABLE 3. Main reference parameters for oblique $\gamma_\infty = 45°$ flat-plate water entry with various angles of attack α.

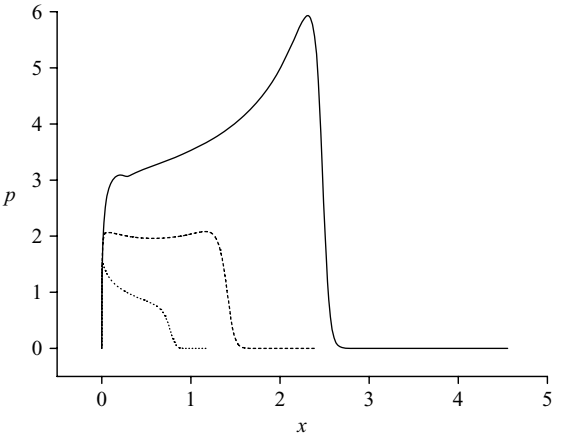

FIGURE 6. Effect of the deadrise angle on the pressure distribution for a flat plate vertically entering the free surface: $\beta = 30°$ (solid line); 45° (dashed line); 60° (dotted line).

Another direction of the horizontal velocity component corresponds to angles $\gamma_\infty > 90°$. Presented in table 4 are the same quantities as in table 3 but for $\gamma_\infty = 135°$. The results obtained show that the contact angle μ_O/π tends to the value 0.25 as $\alpha \to 0$. This value corresponds to the maximum value of the contact angle obtained from the theoretical estimation made by Dobrovol'skaya (1969) and Fraenkel & Keady (2004) for symmetric wedge water entry. However, the actual maximum value in this case obtained by these authors is $\mu_O/\pi = 0.1$. This difference may be due to the geometric constraint on the maximum value of the deadrise angle, which is 90° for symmetric wedge entry, while for our case it is 180°. From the results in table 4 it can also be seen that the angle at the tip of the splash jet $\mu_B \to \gamma_\infty = 135°$ as $\alpha \to 0$ just as it does for the other velocity directions γ_∞ discussed above. However, in this case it rapidly decreases if the angle of attack slightly increases.

In figure 8, streamline patterns are shown for several conditions of oblique flat-plate water entry. The stagnation point moves from the leading edge along the plate as the angle of attack $\alpha = \gamma_\infty - \beta$ increases. The case of a small deadrise angle like that shown in figure 8(d) may occur for surf-planing along a rising wave. The pressure distributions along the plate for figures 8(a) and 8(d) are shown in figure 9. These have

α	β	μ_O/π	μ_B/π	y_O	y_B	p_A	C_n
0.01	134.99	0.250	0.741	0.000	0.000	1.00	0.43
0.1	134.9	0.245	0.659	0.003	0.001	1.00	0.43
1	134	0.217	0.435	0.025	0.005	1.01	0.44
5	130	0.168	0.348	0.124	0.022	1.04	0.49
10	125	0.139	0.325	0.248	0.043	1.09	0.57
20	115	0.104	0.304	0.499	0.080	1.19	0.74
30	105	0.081	0.291	0.749	0.117	1.30	0.94
40	95	0.064	0.281	0.987	0.154	1.44	1.17
50	85	0.051	0.271	1.208	0.193	1.60	1.46
60	75	0.040	0.263	1.397	0.234	1.79	1.80
70	65	0.031	0.254	1.549	0.305	2.03	2.23
80	55	0.023	0.246	1.658	0.359	2.35	2.78
90	45	0.016	0.239	1.704	0.464	2.79	3.49
100	35	0.011	0.233	1.745	0.541	3.59	4.97
110	25	0.006	0.226	1.659	0.624	4.68	6.59
120	15	0.002	0.220	1.500	0.766	7.19	10.0

TABLE 4. As table 3 but $\gamma_\infty = 135°$.

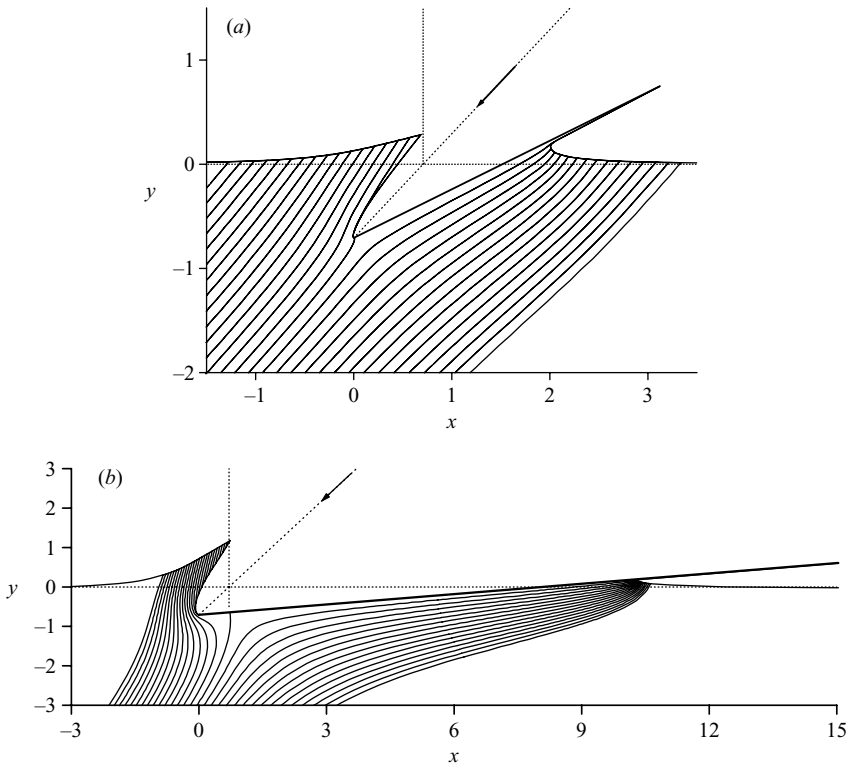

FIGURE 7. Free streamline patterns for oblique flat-plate water entry with $\gamma_\infty = 45°$ for two deadrise angles: (*a*) $\beta = 25°$; (*b*) $\beta = 5°$.

two maxima due to the flow unsteadiness discussed at the end of § 2. The location of the local minimum corresponds to the stagnation point. The larger maximum is caused by the slamming effect occurring near the core of the tip jet. The other

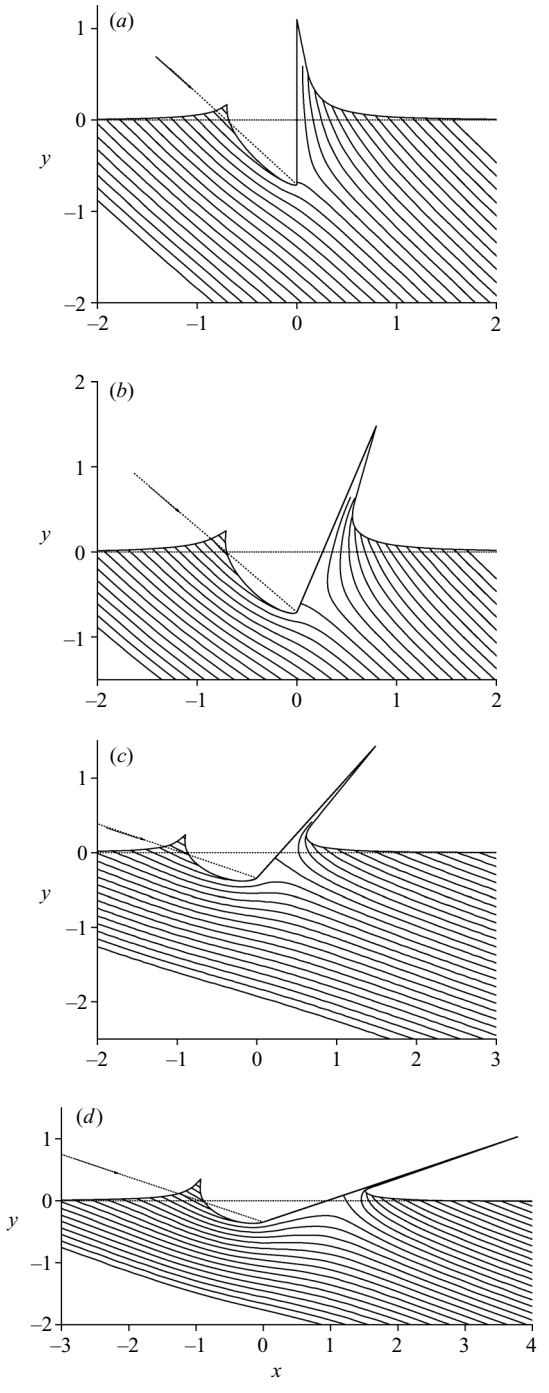

FIGURE 8. Free streamline patterns for oblique flat-plate water entry: (*a*) $\gamma_\infty = 135°$, $\beta = 90°$; (*b*) $\gamma_\infty = 135°$, $\beta = 70°$; (*c*) $\gamma_\infty = 160°$, $\beta = 40°$; (*d*) $\gamma_\infty = 160°$, $\beta = 20°$.

maximum occurs due to the local minimum at the stagnation point since the sign of the pressure gradient changes at this point. A similar but much smaller effect in the pressure distribution near the stagnation point was predicted by Semenov & Iafrati

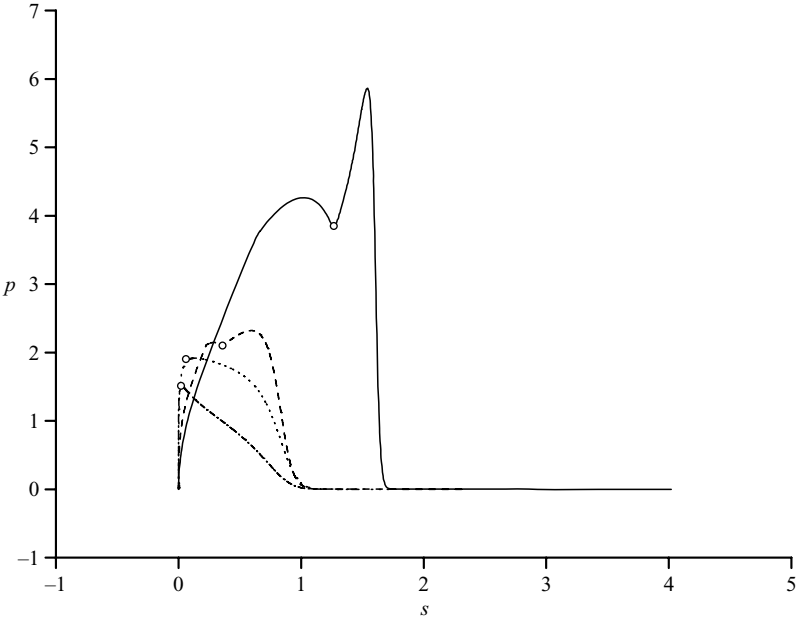

FIGURE 9. Pressure distributions along the plate for cases (*a*) (dash dotted line), (*b*) (dotted line), (*c*) (dashed line) and (*d*) (solid line) in figure 8. The open circles show the pressure at the stagnation points.

(2006) for the vertical entry of asymmetric wedges. For the case of oblique entry, the increase in the pressure peak near the tip jet may occur due to the x-component of the entry velocity causing more liquid to enter the tip jet. Thus the larger the slamming effect, the more visible the effect of the pressure minimum at the stagnation point.

5. Conclusions

We have presented an analytical solution to the nonlinear self-similar problem of flat-plate water entry. The method of the solution is based on some advances in solving two-dimensional boundary-value problems using the calculus of complex variables. Two integral formulae, which determine an analytical function from its modulus and argument given on the real and the imaginary axes of the first quadrant chosen as the parameter region, are presented. These formulae provide the possibility of finding the governing functions of the solution which conformally map the first quadrant onto the complex velocity and complex potential planes without recourse to Chaplygin's singular point method. An analytical expression for the function mapping the parameter region onto the physical plane is found using these governing functions and the flow self-similarity.

Numerical results are presented for a wide range of angles of attack and entry velocity directions. Particular attention is paid to the splash jet occurring on the free surface. It is found that the maximum value of the angle at the tip of the splash jet tends to the value of the deadrise angle as the angle of attack tends to zero. It is also found that at the tip of the splash jet the x-component of the velocity relative to the point at which the leading edge touched the free surface at time $t = 0$ is equal to zero for various initial conditions.

Another new feature is found at the intersection of the free surface and the flat plate for deadrise angles larger than 90°. The contact angle obtained for deadrise angle $\beta \approx 135°$ and angle of attack $\alpha \approx 0$ is about 45°, which is the maximum given by the theoretical estimation obtained earlier (Dobrovol'skaya 1969; Fraenkel & Keady, 2004). We note that the predicted maximum value for symmetric wedge entry is only 18° for a near-zero wedge angle.

For small deadrise angles and large oblique angles of the entry velocity, the pressure distribution along the plate has two maxima with a local minimum between them located at the stagnation point in terms of the self-similar solution.

Parametric dependences of the contact angle, angle at the tip of the splash jet, pressure distribution along the plate and force coefficient have been presented for a wide range of the initial conditions.

REFERENCES

Chaplygin, S. A. 1910 *About Pressure of a Flat Flow on Obstacles. On the Airplane Theory*. Moscow University, 49 pp.

Chekin, B. S. 1989 The entry of a wedge into incompressible fluid. *Prikl. Mat. Mekh.* **53**, 300–307.

Cointe, R. & Armand, J.-L. 1987 Two-dimensional water-solid impact. *ASME J. Offshore Mech. Arc. Engng* **109**, 237–243.

Dobrovol'skaya, Z. N. 1969 Some problems of similarity flow of fluid with a free surface. *J. Fluid Mech.* **36**, 805–829.

Faltinsen, O. M. 2005 *Hydrodynamics of High-speed Marine Vehicles*. Cambridge University Press, 454 pp.

Faltinsen, O. M., Landrini, M. & Greco, M. 2004 Slamming in marine applications. *J. Engng Maths* **48**, 187–217.

Fraenkel, L. E. & Keady, G. 2004 On the entry of a wedge into water: The thin wedge and an all-purpose boundary-layer equation. *J. Engng Maths* **48**, 219–252.

Green, A. E. 1935 The gliding of a plate on a streem of finite depth. *Proc. Camb. Phil. Soc.* **31**, 589–603.

Gurevich, M. I. 1965 *Theory of Jets in Ideal Fluids*. Academic.

Helmholtz, H. 1868 Ueber discontinuirliche Flussigkeitsbewegungen. *Monasber. Berlin Akad.* pp. 215–228.

Howison, S. D., Ockendon, J. R. & Wilson, S. K. 1991 Incompressible water-entry problems at small deadrise angles. *J. Fluid Mech.* **222**, 215–230.

Howison, S. D., Ockendon, J. R. & Oliver, J. M. 2004 Oblique slamming,planning and skimming. *J. Engng Maths* **48**, 321–337.

Iafrati, A. & Korobkin, A. A. 2004 Initial stage of flat plate impact onto liquid free surface. *Phys. Fluids* **16**, 2214–2227.

Mei, X., Liu, Y. & Yue, D. K. P. 1999 On the water impact of general two-dimensional sections. *Appl. Ocean Res.* **21**, 1–15.

Needham, D. J., Billingham, J. & King, A. C. The initial development of a jet caused by fluid, body and free surface interaction. Part 2. An impulsive moved plate. *J. Fluid Mech.* **578**, 67–84.

Oliver, J. M. 2007 Second-order Wagner theory for two-dimensional water-entry problems at small deadrise angles. *J. Fluid Mech.* **572**, 59–85.

Semenov, Yu. A. & Cummings, L J. 2006 Free boundary Darcy flows with surface tension: Analytical and numerical study. *Eur. J. Appl. Maths* **17**, 607–631.

Semenov, Yu. A. & Iafrati, A. 2006 On the nonlinear water entry problem of asymmetric wedges. *J. Fluid Mech.* **547**, 231–256.

Shorygin, O. P. 1995 Hydrodynamics of self-similar flows with internal free surface. *Proc. TsAGI* 2595.

WAGNER, H. 1932 Über Stoßund Gleitvorgänge an der Oberfläche von Flüssigkeiten. *Z. Angew. Math. Mech.* **12**, 192–215.

WANG, D. P. 1977 Water entry and exit of a fully ventilated foil. *J. Ship Res.* **21**, 44–68.

WANG, D. P. 1979 Oblique water entry and exit of a fully ventilated foil. *J. Ship Res.* **23**, 43–54.

WILSON, S. K. 1989 The mathematics of ship slamming. DPhil thesis, Oxford University.

ZHAO, R. & FALTINSEN, O. 1993 Water-entry of two-dimensional bodies. *J. Fluid Mech.* **246**, 593–612.

ZHUKOVSKII, N. E. 1890 Modification of Kirchoff's method for determination of a fluid motion in two directions at a fixed velocity given on the unknown streamline. *Math. Coll.* **15**, 121–278.